Evaluation of infrasound signals from the shuttle Atlantis using a large seismic network

Catherine D. de Groot-Hedlin, Michael A. H. Hedlin, and Kristoffer T. Walker
Institute of Geophysics and Planetary Physics, Scripps Institution of Oceanography, La Jolla, California 92093-0225

Douglas P. Drob
Space Sciences Division, Naval Research Laboratory, 4555 Overlook Avenue, SW, Washington, DC 20375

Mark A. Zumberge
Institute of Geophysics and Planetary Physics, Scripps Institution of Oceanography, La Jolla, California 92093-0225

(Received 6 December 2007; revised 10 June 2008; accepted 11 June 2008)

Inclement weather in Florida forced the space shuttle "Atlantis" to land at Edwards Air Force Base in southern California on June 22, 2007, passing near three infrasound stations and several hundred seismic stations in northern Mexico, southern California, and Nevada. The high signal-to-noise ratio, broad receiver coverage, and Atlantis' positional information allow for the testing of infrasound propagation modeling capabilities through the atmosphere to regional distances. Shadow zones and arrival times are predicted by tracing rays that are launched at right angles to the conical shock front surrounding the shuttle through a standard climatological model as well as a global ground to space model. The predictions and observations compare favorably over much of the study area for both atmospheric specifications. To the east of the shuttle trajectory, there were no detections beyond the primary acoustic carpet. Infrasound energy was detected hundreds of kilometers to the west and northwest (NW) of the shuttle trajectory, consistent with the predictions of ducting due to the westward summer-time stratospheric jet. Both atmospheric models predict alternating regions of high and low ensonifications to the NW. However, infrasound energy was detected tens of kilometers beyond the predicted zones of ensonification, possibly due to uncertainties in stratospheric wind speeds.
 [DOI: 10.1121/1.2956475]

PACS number(s): 43.28.Fp, 43.28.Mw, 43.20.Dk [VEO] Pages: 1442–1451

I. INTRODUCTION

A primary goal in infrasound research is to accurately model transmission of low frequency acoustic energy to distances of several hundreds to thousands of kilometers—a challenging task given that the propagation characteristics are a function of the background winds and atmospheric temperatures, which may vary considerably in space and time (Drob *et al.*, 2003). Unlike in seismology, where Earth's velocity structure is largely derived from the travel times of many intersecting seismic waves, the time dependent atmospheric models used for infrasound propagation modeling are not derived from direct recordings of sound waves, so there is no assurance that they will yield predictions that agree with observations. Infrasound studies are thus inextricably linked to the atmospheric sciences, as diverse data sets ranging from direct observations to climatological models provide the specifications of the sound and wind speed profiles required for modeling infrasound propagation. An inability to accurately model a set of infrasound observations indicates a knowledge gap in our understanding and ability to specify the state of the atmosphere. Recently, studies have demonstrated the utility of infrasound research to advance scientific understanding of the atmosphere (see, e.g., Le Pichon *et al.*, 2002; Millet *et al.*, 2007; and Arrowsmith *et al.*, 2007).

The objective of this paper is to use observations to evaluate our ability to model low frequency sound propagation through the atmosphere for a single ground-truth event. This relies on our knowledge of the atmosphere at the time of the event, the infrasound source, as well as the physical assumptions used in propagation modeling. Until recently, there have been limited opportunities to evaluate present-day atmospheric models using infrasound signals from sources for which we know exactly when and where the source occurred. The recent re-entry of the space shuttle Atlantis over the heavily instrumented western United States provided one such opportunity. Although the shuttle usually lands at the Kennedy Space Center (KSC) in Florida, severe weather in the vicinity of KSC on June 22, 2007 forced NASA to direct Atlantis to the alternate landing site at Edwards Air Force Base (AFB) in the Mojave Desert in southern California. A time and position record of its trajectory was recorded with an onboard GPS receiver. On its approach to Edwards AFB, the shuttle passed just west of Baja California and then across San Diego and Los Angeles before passing below the sound barrier just above the Mojave Desert. A double sonic boom was heard by millions of people and, fortunately for this study, was recorded by over 100 three-component seismic stations of the USArray (Meltzer *et al.*, 1999), various regional seismic networks, and three infrasound arrays in

southern California and western Nevada. The temporary presence of the transportable USArray in this region provides this study with a much broader and denser array of sensors than would have otherwise been available. Although seismic wave forms do not yield an accurate measure of the infrasound amplitude or structure due to local variations in the efficiency of air to ground coupling, they can provide both travel times and a lower limit on the ground exposure to the sonic boom.

Previous studies involving seismic recordings of shock waves include using arrival times to estimate a rough trajectory of supersonic objects including a bolide (Ishihara *et al.*, 2004; Langston, 2004) and the space shuttle Columbia (Kanamori *et al.*, 1992). Wave form characteristics have been used to estimate the seismic velocity of near-surface layers (Langston, 2004) and to infer mechanisms by which ground roll is excited (Kanamori *et al.*, 1991, 1992). These studies made use of a constant sound speed to model acoustic propagation through the atmosphere. This approximation is generally adequate for sound propagation to the primary sound carpet, which is associated with downward propagation of sound from supersonic objects to the ground and has a width of tens of kilometers. It can also be accurate to first order at greater distances; Cochran and Shearer (2006) employed a constant acoustic velocity to infer the location of explosive sources recorded at seismic networks in Southern California, and Gibbons *et al.* (2007) applied joint seismic-infrasound processing to arrivals recorded at small seismic arrays to find the direction of arrival of explosive sources.

An accurate description of the atmospheric state is required to model propagation at greater lateral distances from the flight trajectory, where arrivals associated with refraction from the stratosphere may form a secondary sound carpet. Ducting between the ground and temperature and wind speed gradients in the lower, middle, and upper atmosphere allows infrasound waves to propagate to distances of hundreds to thousands of kilometers. Concorde flights have been recorded at infrasound sensors at distances from hundreds to thousands of kilometers (Le Pichon *et al.*, 2002; Liszka, 1978); however, in a previous study, Cates and Sturtevant (2002) showed that ray-tracing through a one-dimensional profile of wind and sound speeds underpredicted the extent of the sonic boom coverage.

The present study focuses on regions of sound exposure to Atlantis' supersonic descent and arrival times for sensors in these areas. We compare observations of infrasound arrivals at seismic and infrasound stations covering a region extending from 31° to 40°N and from −112° to −124°W with predictions based on ray-tracing through a detailed three-dimensional (3D) atmospheric model. Our aim is to evaluate the success of atmospheric models and ray-based infrasound propagation modeling in predicting the observations.

The atmospheric specifications, seismic network availability, and shuttle trajectory data for this study are discussed in Sec. II. A model of sound excitation by a supersonic object, as well as the subsequent transmission of infrasonic waves through a realistic windy atmosphere, are described in Sec. III. This is followed by a description of seismic and infrasound recordings of the Atlantis re-entry. The model predictions are compared to the observations in Sec. V, and we conclude with a discussion about the implications of our observations to the accuracy of the atmospheric models.

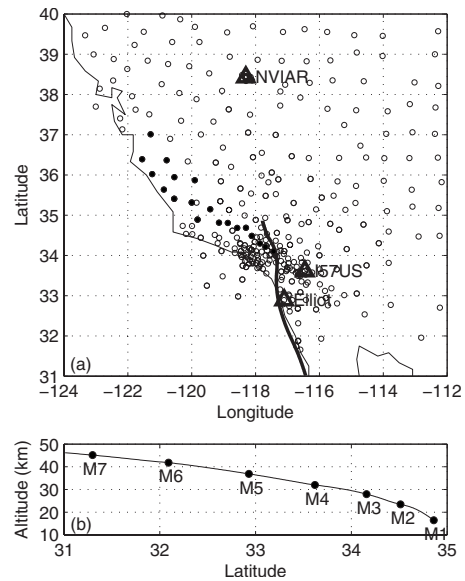

FIG. 1. (a) Map of the study area showing stations and the shuttle's path. Infrasound stations are represented by triangles and labeled. Seismic stations are represented by small circles. Wave forms of stations marked by filled circles are plotted in Fig. 8. The supersonic portion of the shuttle trajectory is shown by the dark solid line. (b) The shuttle altitude as a function of latitude is shown with associated Mach numbers.

II. DATA AND ATMOSPHERIC SPECIFICATIONS

This study combines a hybrid atmospheric specification at the time of the shuttle's re-entry with seismic and infrasound wave forms recorded on the ground and detailed telemetry on the shuttle itself.

A. Seismic data

Several seismic networks were operating in southern California, Nevada, and Mexico during the re-entry (Fig. 1). The most extensive network was the USArray (Meltzer *et al.*, 1999), which comprised over 300 stations and operated continuously through the re-entry. Deployment of the transportable stations within this array began in 2005 in southern California, and stations are scheduled to be removed in late 2007 for redeployment elsewhere. The June 22 re-entry of Atlantis is the only space shuttle landing that occurred in southern California during this time period. The ten-element NVAR seismic network in Nevada operated as part of USArray and is located 400 km north of the point at which the shuttle passed below Mach 1. NVAR has an aperture of 5 km. Several stations in northern Baja California were available as well as continuous and triggered stations operated by the California Institute of Technology (Caltech, Pasadena, CA). Ground velocity was recorded at between 20 and 100 Hz on three components by most stations in these networks. In total, there were about 350 stations operating within the study area.

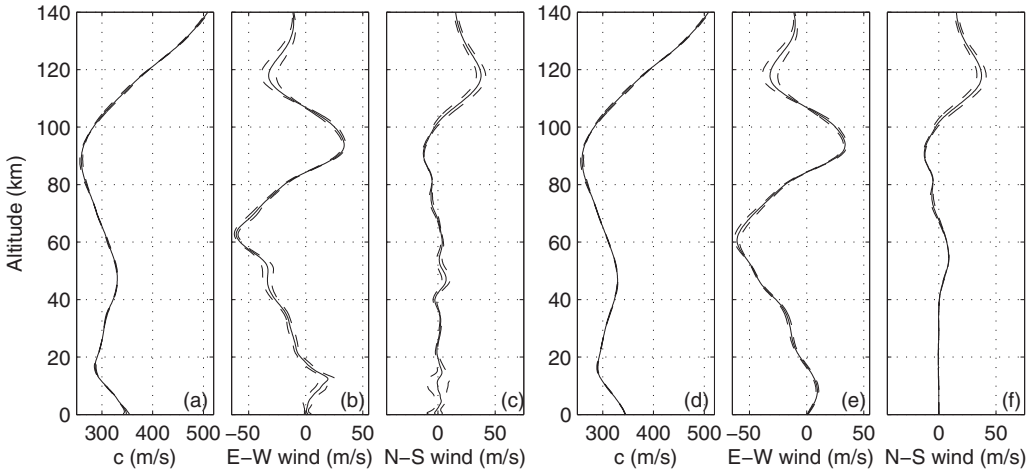

FIG. 2. (a) The mean sound speed as a function of altitude over the study area is shown by the solid line for the G2S model. The variability in the sound speeds over the study region is shown by the dashed lines, which indicate +/− one standard deviation in sound speeds at each altitude. (b) The mean zonal wind speed profile (positive eastward) over the same region is shown by the solid line, with the variability in values over the study region shown by the dashed lines. (c) Same as for (b) but for the mean meridional wind speed profile (positive northward). (d)–(f) show the corresponding values based on climatology data only.

B. Infrasound data

Infrasound stations located at Camp Elliott (collocated with seismic station 109C just northeast of San Diego), Anza-Borrego desert (I57US), and Nevada (NVIAR) recorded infrasound from the re-entry [Fig. 1(a)]. NVIAR was the only station to record the signals on enough array elements to determine the direction to the source. NVIAR is also colocated with the inner elements of the NVAR network and has an aperture of 1.6 km. The infrasound instrumentation at Camp Elliott [optical fiber infrasound sensor (OFIS)] is unique in that it uses fiber optic laser interferometry to resolve minute changes in pressure while reducing incoherent wind noise and turbulence by averaging pressure along a line (Zumberge *et al.*, 2003). The sensor has a flat instrument response from 0.01 to 100 kHz, so it is ideally suited to record an *N*-wave. The OFISs were not arranged in an array configuration at the time of the re-entry.

C. Shuttle telemetry

Shuttle trajectory data consist of a series of coordinated universal time (UTC) times and associated coordinates in the Earth centered Earth fixed reference system reported at 1 s intervals from over the Indian Ocean to the landing at Edwards AFB. These coordinates were converted to latitude, longitude, and altitude in the WGS-84 reference frame. The speed of the shuttle decreased from approximately Mach 6 near the United States-Mexico border to subsonic just south of Edwards AFB. The altitude decreased from over 40 km at Mach 6 to 16 km at Mach 1 [Fig. 1(b)]. There is a small error in the position reported by the GPS receiver located in the shuttle cockpit due to plasma effects. The 67% location uncertainty over the study area ranged from less than 25 m to less than 50 m.

D. Atmospheric specifications

The Naval Research Laboratory (NRL) ground to space (G2S) model of Drob *et al.* (2003) was used to provide background sound speeds and wind fields from 31°N to 40°N and from −124°W to −112°W, for 18:00 GMT, June 22, 2007. The G2S data processing system combines available global operational atmospheric numerical weather data from the National Oceanic and Atmospheric Administration Global Forecast System (NOAA-GFS) and the National Aeronautics and Space Administration Goddard Earth Observing System (Versions 4) (NASA-GEOS4) system (e.g., Kanamitsu, 1989; Kalnay *et al.*, 1990; Bloom *et al.*, 2005) with the NRL mass spectrometer, incoherent scatter model, 2000 version, horizontal wind model, 1993 version (NRL MSISE-00/HWM-93), and upper atmospheric empirical models (Picone *et al.*, 2002, Hedin *et al.*, 1996). The G2S model merges these data via a vector spherical harmonic transform and function fitting methodology between altitudes from the surface to approximately 250 km. The horizontal information content of the hybrid specifications varies from $1° \times 1°$ resolution in the lower atmosphere to $5° \times 5°$ resolution in the upper atmosphere. In the vertical direction the resolution varies from 350 m to a few kilometers in the upper atmosphere. Single point inverse vector spherical harmonic transforms combine with cubic spline interpolation to synthesize arbitrarily defined 3D data cubes of the winds and adiabatic sound speed fields in altitude coordinates at any desired output resolution.

The vertical sound and wind speed profiles extend up to an altitude of 140 km from the resulting G2S hybrid specification plus the corresponding NRL MSISE-00/HWM-93 climatological models (Fig. 2). To first order the primary aspects of the infrasound propagation characteristics are governed by the local vertical gradients of atmospheric fields (Drob *et al.*, 2003). The variability in sound and wind speeds over the study region for each model is indicated by the dashed curves. The ambient horizontal wind and sound speed gradients have a second order influence on the propagation; however, when integrated over long distances (greater than 500 km), significant changes in the local vertical structure cannot always be ignored (Drob *et al.*, 2003).

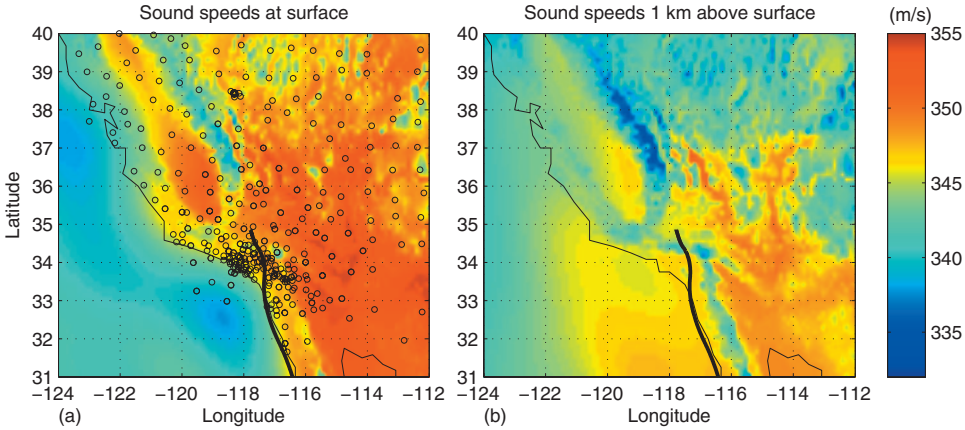

FIG. 3. (a) Sound speeds from G2S atmospheric data on the surface and (b) at a height of 1 km above the ground. Also shown are station locations and the shuttle trajectory down to Mach 1. NVAR is the dense collection of stations near 38°N and 118°W. The increase in sound speed with altitude over the ocean indicates the presence of a marine inversion layer.

Atmospheric specifications based on both models indicate that during the time of the event the adiabatic sound speeds at low altitudes are greater than those within the stratosphere. Thus adiabatic sound speed gradients alone are insufficient to cause sound to be refracted to the ground. At midlatitudes, the efficiency of stratospheric ducting is strongly influenced by seasonally varying zonal winds. During the time of this event, the zonal winds are reasonably strong to the west near the stratopause, approaching 60 m/s at an altitude of 60 km. Thus the effective sound speed (the adiabatic sound speed plus the wind speed in the direction of propagation) is increased for propagation to the west but decreases for propagation to the east. Therefore stratospheric ducting is predicted only for propagation to the west. Acoustic refractions from the large sound speed gradients in the thermosphere are also predicted. However, they are typically observed only for large events or for sensitive infrasound sensors (e.g., Balachandran *et al.*, 1977) since acoustic absorption increases with altitude and frequency (Sutherland and Bass, 2004).

As mentioned, in some instances range dependence can also be important in determining the infrasound propagation characteristics from source to receiver. A more detailed view of the G2S atmospheric model for this date and time is shown in Fig. 3 for sound speeds at the surface and at a height of 1 km. The marine inversion layer over the Pacific Ocean does not exist over the land mass, and infrasound may scatter into or out of this duct at the boundary.

III. SOURCE AND INFRASOUND PROPAGATION MODELS

The motion of a solid object through the atmosphere displaces air, causing a pressure disturbance that travels at the local sound speed. Pressure waves interfere constructively near any supersonic object, which creates a shock wave with a shape that depends on the object's geometry and speed (Whitham, 1974). Nonlinear effects near the shuttle cause the acoustic waves to steepen, which results in the characteristic *N*-wave generated by supersonic aircraft. The pressure disturbance propagates at right angles to the shock wave front near the aircraft. At greater distances, the pressure disturbance propagates acoustically with sound transmission governed by winds and sound speed gradients in the atmosphere.

Our model relies on the assumption that the shock wave governs only the allowable initial propagation angles and that the subsequent propagation of acoustic energy is linear from the shuttle trajectory to receivers on the ground. Linear propagation implies that the magnitude of the pressure perturbation due to the passage of the sound wave is very small compared to the ambient pressure. Under this approximation, the sound speed is independent of the pressure amplitude, and standard acoustic propagation methods may be used to model the sound transmission; here, we use ray-tracing methods. For Atlantis, which has a slender conically shaped nose, we make the standard assumption that the shock wave front may be represented as a cone with a half-angle of $\alpha = \sin^{-1}(c/v)$ where c is the sound speed and v is the shuttle velocity. The shuttle trajectory and the Mach cone angle α thus define the initial propagation direction for the acoustic wave front at any given point along the shuttle's trajectory. We assume that the shape of the cone, as well as the initial propagation direction, is not significantly affected by the winds along the shuttle's path or the shape of the shuttle's nose. A similar approach was used by Cates and Sturtevant (2002).

We approximate the source as a distribution of Mach cones at points along the shuttle trajectory, as in (Le Pichon *et al.*, 2002). Each source point is offset by location and time as determined from the telemetry data. For a coordinate system in which Atlantis travels horizontally and directly northward, allowable grazing angles, g, for rays perpendicular to the Mach cone are defined by

$$g = \sin^{-1}(\cos\alpha \cos\beta),$$

where g is defined as positive upward with respect to the horizontal axis and β is the interior angle within the Mach cone, measured clockwise from vertical as shown in Fig. 4. Feasible grazing angles for rays perpendicular to the Mach cone range from $-\cos^{-1}(c/v)$ to $+\cos^{-1}(c/v)$ at any given point along the shuttle's path. The corresponding ray azimuth with respect to north is given by

$$\theta = \sin^{-1}(\cos\alpha \sin\beta/\cos g).$$

The azimuths and grazing angles for a more general shuttle trajectory are derived by 3D coordinate rotation using the shuttle's azimuth and angle of descent at each point.

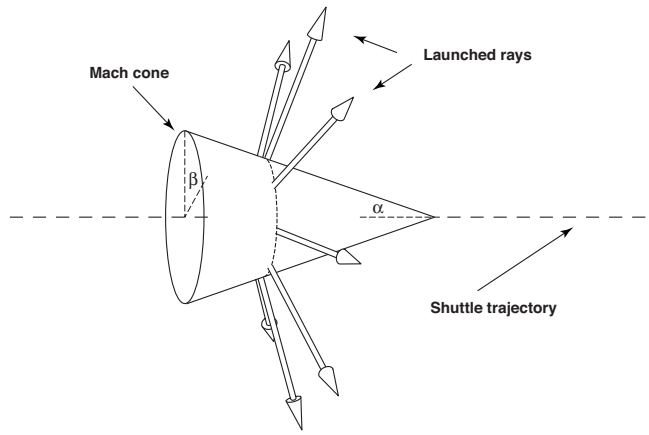

FIG. 4. Rays are launched at right angles to the Mach cone. The Mach cone angle α and interior angle β are indicated.

Each ray is launched at a right angle to the Mach cone (Fig. 4), at a position given by the shuttle's GPS receiver, and is propagated through the G2S model according to acoustic refraction laws in a windy atmosphere; these laws obey Fermat's principle of least time in an advected medium (Thompson, 1972; Ostashev *et al.*, 2001). Our ray method allows for both vertical and lateral variations in adiabatic sound speeds and winds, as well as reflection points along Earth's surface. Rays are launched at even increments in β, the interior cone angle.

Longitudinal propagation through the G2S model is illustrated in Fig. 5 for a single point on the shuttle's trajectory, not taking into account cone geometry. For illustration, we make the assumption that the ground surface along this profile is flat and at sea level elevation. We also have not considered rays that turn in the thermosphere above 120 km. Points west of 119°W lie over the Pacific Ocean. Rays are initiated within the vertical plane over a series of angles relative to the horizontal ranging from directly down to directly up. Black lines illustrate rays with end points on the ground.

As shown in Fig. 5, steeply downward-going rays from the shuttle form a primary sound carpet across both directions. There is no ducting of infrasound energy between the ground and upper atmosphere for propagation to the east due to the presence of the westward summer-time stratospheric jet. For westward propagation, rays launched at shallow upward angles refract from the stratosphere back to the ground to form a secondary sound carpet. Multiple refractions and reflections between the stratosphere and the ground, and within the lowest 1 km of the troposphere, carry the sound farther from the source. The lower panel of Fig. 5 illustrates the reduced travel times corresponding to these rays. Rays are launched at uniform intervals; thus, the G2S atmospheric specifications for this event predict far fewer rays, and hence lower infrasonic levels, between the primary carpet and the first westward propagating stratospheric arrivals. Farther from the source, some of the energy originally ducted between the ground and stratosphere becomes trapped in a marine inversion layer over the Pacific Ocean. This inversion layer has the effect of increasing infrasound levels at the surface. The lower panel of Fig. 5 illustrates multiple arrivals for points west of 120.2°W. The separate arrivals imply that acoustic phase velocities associated with stratospheric ducting arrive later than for tropospheric ducting. Consequently, later arrivals are associated with acoustic energy that has been stratospherically ducted over a greater portion of the travel path.

Multipathing and acoustic shadow zones are further investigated in Fig. 6. Results from atmospheric specifications based on the G2S model and the standard climatology are shown. End points at which the rays reached the sea level reference surface are marked by dots. Rays were launched at equal increments of 0.2° over the interior of the Mach cone and at 6 s intervals along the shuttle path, so regions where the density of points is low between direct and stratospheric arrivals suggest low infrasound levels. Acoustic shadow zones exist beyond the primary sound carpets to the east of the shuttle trajectory and to the NW of the landing point. As shown, the ray propagation method predicts a sharp edge to the primary sound carpet east of the shuttle transit path for both sets of atmospheric specifications. The transition is less pronounced to the west due to stratospheric and tropospheric ductings. The G2S model predicts that tropospheric ducting

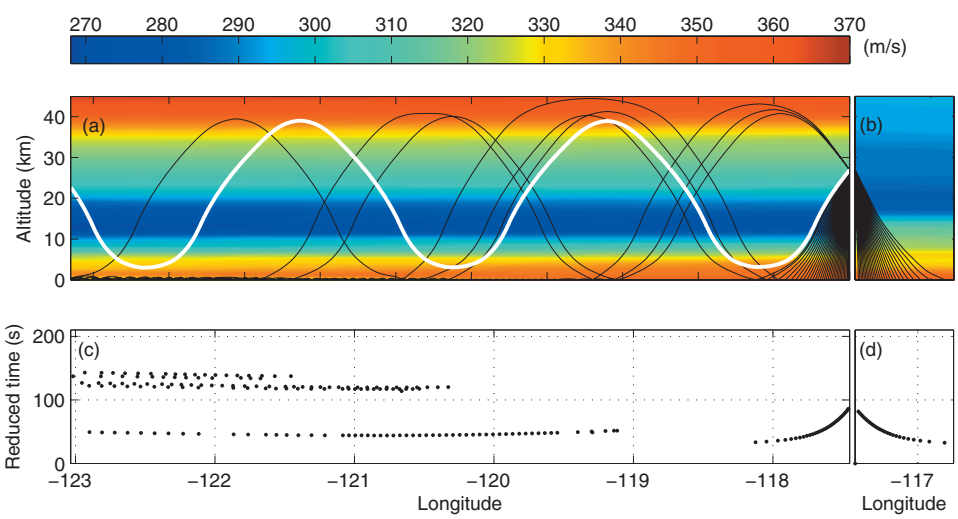

FIG. 5. (a) Ray paths from 34.25°N and 118.5°W for propagation to the west. The white line indicates one of the many ray paths that do not reach the ground. Background colors indicate the effective sound speed, given by the sum of the adiabatic sound speed and the wind velocity in the direction of propagation. Note that these are equal to sound speeds in an advected medium only for horizontal propagation. (b) Rays for propagation to the east. Identical color scales are used in (a) and (b). (c) Reduced travel times for propagation to the west and (d) east. Reduced travel times are given by $(t-|r|/v_r)$ as a function of longitude, where t is the travel time in seconds along the ray path, $|r|$ is the range from the source, and v_r is the reducing velocity, set to v_r=335 m/s here.

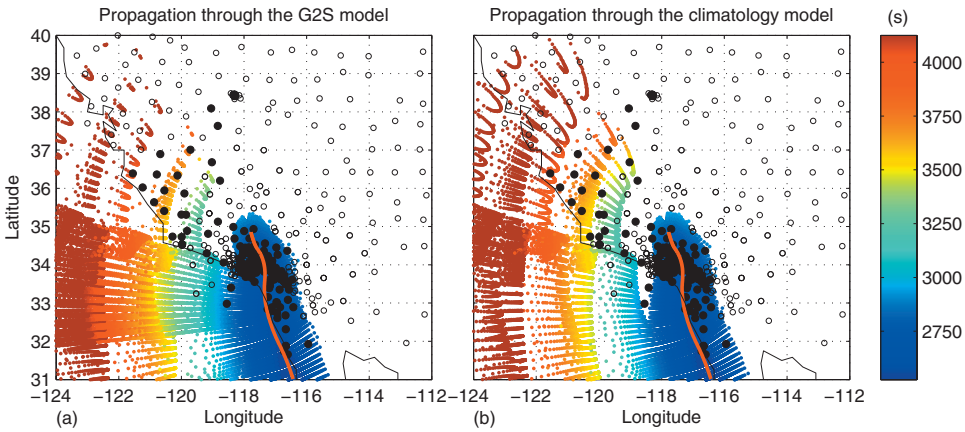

FIG. 6. Maps of ray end points that reach the ground, for rays starting along the supersonic portion of the shuttle trajectory, are shown in red. We have ignored rays that turn in the thermosphere above 120 km; these would arrive significantly later for stations located over 250 km from the shuttle path. The rays were propagated through atmospheric specifications provided by the (a) G2S model and by (b) climatology data. The end points are color-coded according to the predicted arrival time in seconds after 1900 GMT. For comparison, the shuttle speed drops below Mach 1 at 2732 s after 1900 GMT. Small circles indicate station locations that did not register detections; filled circles indicate stations that recorded an arrival. Rays were launched at even intervals, so regions where ray densities are low indicate either low infrasound levels (e.g., regions between stratospheric arrivals) or acoustic shadow zones (beyond the primary carpets to the east and north).

is significant only over the ocean; the climatology predicts only stratospheric returns. Shadow zones are predicted farther to the north-NW for the atmospheric model based on climatology. Note that these differences arise from relatively small differences in the wind profiles at altitudes of less than 60 km, as indicated in Fig. 2.

IV. OBSERVATIONS

The observations for this paper are based on continuous and triggered recordings made at over 130 seismic stations distributed across the study area as well as continuous recordings made at 3 infrasound stations. We have divided our recordings into two classes. Near-field recordings were made by infrasound and seismic stations located beneath the shuttle or immediately to the side (within about 100 km of the shuttle on its closest pass). Acoustic energy propagated directly downward from the shuttle to these stations. Therefore signals at these stations can be unambiguously associated with the shuttle. At greater distances, it was more difficult to associate acoustic signals at seismic stations with the shuttle's passage as station density in the outlying areas was lower.

A. Near-field recordings

The shuttle was recorded by 109 seismic stations and 2 infrasound stations located in a 200 km wide corridor beneath Atlantis north of the United States-Mexico border. Many of the seismic recordings show a remarkable degree of similarity even though they recorded the shuttle at speeds ranging from over Mach 5 down to Mach 1 at distances ranging from 0 to over 80 km east and west of the shuttle's track [Fig. 1(a)]. Associating acoustic arrivals from the shuttle at these stations was straightforward for a couple of reasons. First, most signals were recorded with a high signal-to-noise ratio (SNR). Second, the station density was high beneath the shuttle from the United States-Mexico border to the point at which the shuttle dropped below Mach 1 near Edwards AFB, permitting us to observe the acoustic phase moving out between stations.

The acoustic signal near the shuttle is an *N*-wave; the equivalent seismic velocity response is a doublet. The seismic station 109C was colocated with OFISs at Camp Elliott near San Diego. Figure 7 shows the OFIS acoustic and adjacent seismic recordings at this location. The *N*-wave is recorded well by the broadband OFIS. The collocated broadband seismometer (STS-2) recorded a modified version of the *N*-wave. Also seen in the recorded seismic velocity is a Rayleigh wave that precedes the acoustic signal at this location. Rayleigh waves have been attributed to acoustic-to-

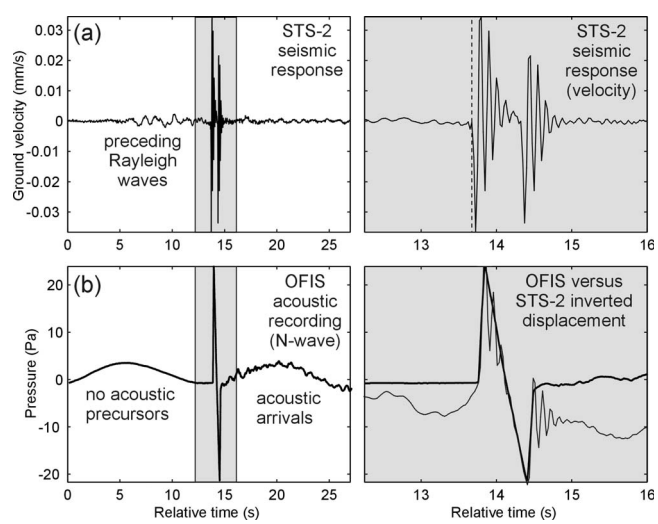

FIG. 7. Comparison between the (a) seismic and (b) infrasound recordings for US Array station 109C (Camp Elliott). The vertical dashed line marks the travel time pick based on the seismic data. The integral of the seismic velocity record is plotted (as the gray line) with the infrasound recording in the lower right panel.

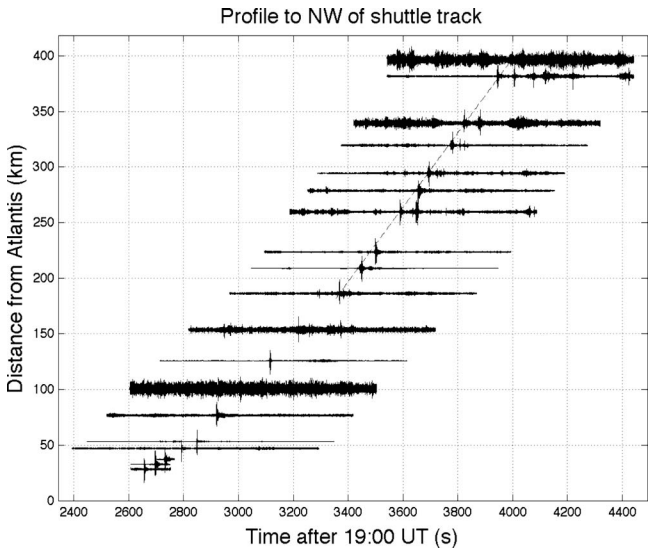

FIG. 8. Bandpassed recordings (2–8 Hz) along a profile to the NW of the shuttle, indicated by filled circles in Fig. 1. The wave forms are plotted as a function of distance from the nearest point on the shuttle path, which was located just south of Edwards AFB where the shuttle slowed to Mach 1. The increasing complexity of recordings past 225 km may indicate multipathing. The dashed line delineates a propagation velocity of 335 m/s.

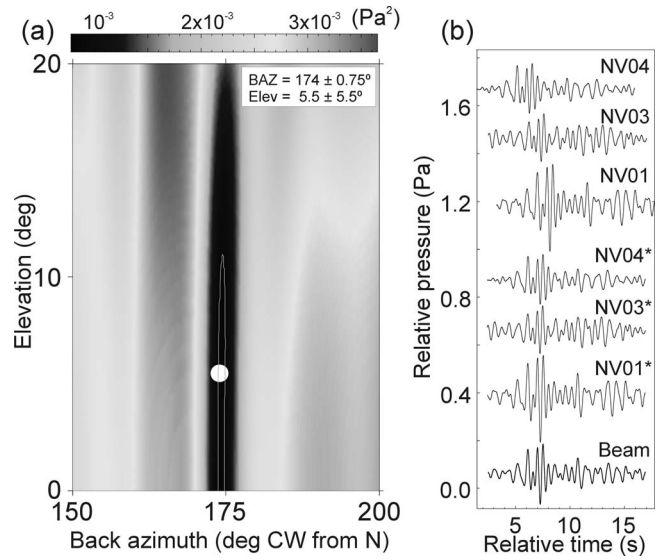

FIG. 9. Time domain beamforming for infrasound station NVIAR, Nevada. A 0.8–3.0 Hz bandpass filter is applied to the data. The array aperture is 1600 m, which can resolve subhorizontal signals down to about 0.1 Hz. (a) The 95% confidence region is outlined by a gray line. (b) The time-shifted wave forms.

seismic coupling near the shuttle (e.g., Kanamori *et al.*, 1991) and are easily distinguished from the infrasound arrival due to their lower frequencies and amplitudes.

B. Distant recordings

Wave form recordings of the shuttle made more than 100 km from the shuttle's path are more structured. Due to longer propagation paths, variable noise levels at the recording stations and the greater spacing between stations, these signals are poorly correlated. Wave forms at these stations are longer in duration and, in some instances, appear as a series of multipathed arrivals. Similar behavior for the seismic observations of the Washington state bolide event was observed (Arrowsmith *et al.*, 2007). To isolate signals from the shuttle at these stations, we plotted recordings as a function of distance of each station from the closest pass of the shuttle. In one example of such a record section, shown in Fig. 8, there is a distinct onset of energy at the distant stations located to the NW of the shuttle's track moving out at a speed of approximately 335 m/s (dashed line). In each case, we picked travel times based on the first onset of the impulsive energy (i.e., after the Rayleigh wave).

Seismic networks can be useful for detecting high amplitude infrasound signals but weaker infrasound signals, or those that propagate subhorizontally, may not generate recognizable seismic phases. For example, the NVIAR infrasound array is located at the edge of the seismic signal detection zone in Nevada and recorded signals (with an average SNR of 16 dB) that were not coherent across the much larger collocated NVAR seismic array.

Although three infrasound signals can be observed on most of the infrasound array, the signals may be obscured by intermittent wind noise. The second signal has the highest SNR. Time domain beamforming is used to estimate the second infrasound signal's back azimuth and elevation angle (Fig. 9). The acoustic wave speed is calculated from the measured air temperature assuming that the winds are negligible. A grid search is applied over trial back azimuth and elevation angle to minimize the sum of squares of the misfit between time-shifted wave forms, permitting a rigorous search of the solution space for local minima. The 95% confidence contour is derived assuming the sum of squares reflects a chi-squared noise process and using the technique of Silver and Chan (1991) to estimate the average number of degrees of freedom for the filtered wave forms. The back azimuth and elevation angle are estimated to be $174 \pm 0.75°$ and $5.5 \pm 5.5°$. This suggests an apparent speed across the array of 351 m/s. At such a low elevation angle, an approximately 10 m/s difference in north-south wind speed is required to explain a 10° inaccuracy in elevation angle. Three incoherent seismic signals are observed across the NVAR array, with energy packets that align along the 351 m/s moveout line (Fig. 10). The outlying elements of NVAR are not shown due to high noise (NV11, NV31) or poor data quality (NV32, NV33). Projection of the back azimuth uncertainty envelope from the middle of the infrasound array defines an 11 km wide swath that blankets Edwards AFB and the Mach 1.0 part of the trajectory. This may suggest that deceleration and consequential flattening of the Mach cone are the sources of the infrasound signals at this location in Nevada.

The detections and arrival times at all stations are summarized in Fig. 11. The accuracy in the arrival times for the near-field stations is less than 0.1 s due to the high SNR, sharp signal onsets, high coherence of the doublet signals between the closely spaced stations, and the acoustic moveout. At the distant stations the signals were highly variable and less defined, resulting in arrival time errors on the order of 0.5–1 s. Stations not highlighted in Fig. 11 did not record a detectable signal.

Many stations beneath the shuttle's track recorded a signal (Fig. 11). To the east, there is a sharp boundary between

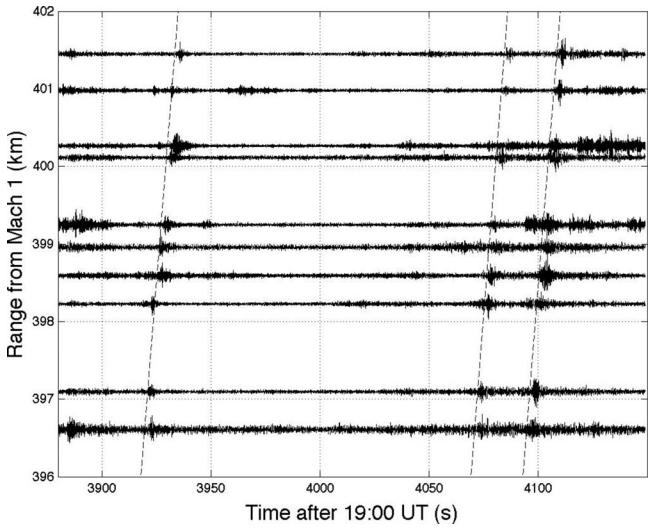

FIG. 10. NVAR seismic signals plotted with respect to time and distance to the point at which the shuttle slowed to Mach 1. The dashed lines have a slope of 352 m/s. These traces were bandpass filtered from 0.5 to 5.0 Hz.

the primary sound carpet and the shadow zone, with no signals observed farther to the east. Stations on two of the five islands to the west recorded signals. Surprisingly, most stations less than 400 km to the NW of the shuttle recorded the event. As discussed earlier, the colocated NVAR seismic network and NVIAR infrasound array approximately 400 km north of Edwards AFB clearly recorded the shuttle. The lack of detections at stations to the NW suggest the presence of regions of low ensonification or a shadow zone although it may be that some stations did not record a signal due to high noise or poor acoustic-to-seismic coupling. Our ability to map out the precise boundary of the shadow zone is also limited by the station density. Finally, it should be noted that the observed arrival times are inconsistent with thermospheric arrivals, which are predicted to arrive later than the stratospheric arrivals. Thermospheric arrivals were not observed in the frequency bands considered by this study.

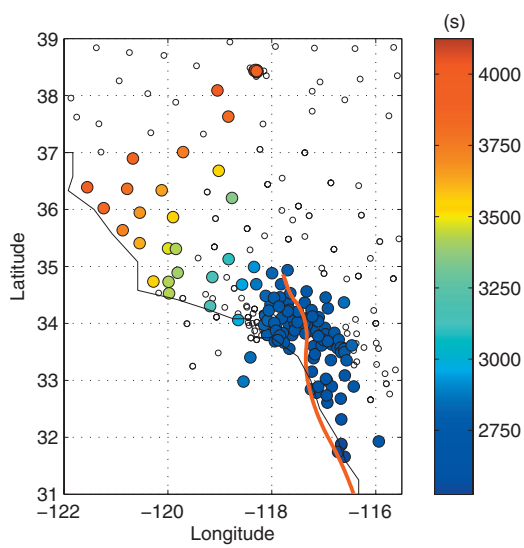

FIG. 11. Map of stations at which infrasound arrivals were detected. The stations are color-coded to show the time of the first arrival in seconds after 1900 GMT. Small circles show where signals were not detected. Compare to Fig. 6, which shows predicted travel times at the same color scale.

V. COMPARISON BETWEEN OBSERVATIONS AND PREDICTIONS

Comparison of Fig. 11 with Fig. 6 indicates qualitative agreement between predictions and observations. First, we predict a sharp edge to the primary acoustic carpet to the east of the shuttle with no propagation after that, in agreement with observations. The atmospheric specifications based on the G2S model predict tropospheric ducting and downward refraction over the ocean to the west, which agrees with the signals observed at the island stations. Ray modeling based on both sets of atmospheric specifications predicts alternating areas of high and low ensonifications over land to the NW, with most stations not in a position to record detectable signals; this conflicts with the detections over a broad region to the NW. We also accurately predict a total absence of signals to the north of Edwards AFB and beyond the primary carpet to the east of the shuttle trajectory. Finally, the 335 m/s moveout velocity, shown in Fig. 8 for arrivals to the NW of the shuttle track, shows close agreement with the predicted moveout speed for arrivals to the west (Fig. 5).

Travel times from the shuttle trajectory to each site were computed in order to make a quantitative comparison between predications and observations. Rays were launched at a greater ray density than illustrated in Fig. 6 to match observation points with predicted travel time. Families of rays with end points within a given radial cutoff distance d_c from the station and with similar travel paths were binned to yield travel times. The cutoff distance d_c was set either to 6 km, or the distance subtended by a 2° angle at a range of $r_{\min}$, whichever is larger, where $r_{\min}$ is the shortest range between the station and shuttle trajectory. We assume that travel times vary with radial distance from source to receiver, and only negligibly with azimuth, over the distance d_c. For each station, we therefore corrected the travel times using a reducing velocity derived from a linear fit to a travel time versus overshoot curve.

Figure 12 shows the time residual between the predicted and observed arrival times, defined here as the predicted minus the observed arrival time. These residuals were computed both for atmospheric specifications. In the context of this discussion it should be noted that there are instances where the actual state of the atmosphere will be close to that of the climatological average, whereas at other times there can be significant departures; for example, during the time and location of the Buncefield oil depot explosion (Evers and Haak, 2007) where stratospheric wind velocities were 120 m/s. As shown in Fig. 2 for this event, the state of the lower and middle atmosphere is close to that of the climatological state. Both models indicate large negative residuals for both sets of atmospheric specifications at a longitude of about 120°W and at latitudes south of 36°N. Predicted arrival times within this region are too early by approximately 80 s. Comparison with the travel time predictions shown in Fig. 6 indicates that, for both atmospheric models, these points lie in a region where ray densities are comparatively low. At the station farthest to the NW (the second trace from the top in Fig. 8), the predicted time lagged the observed time by

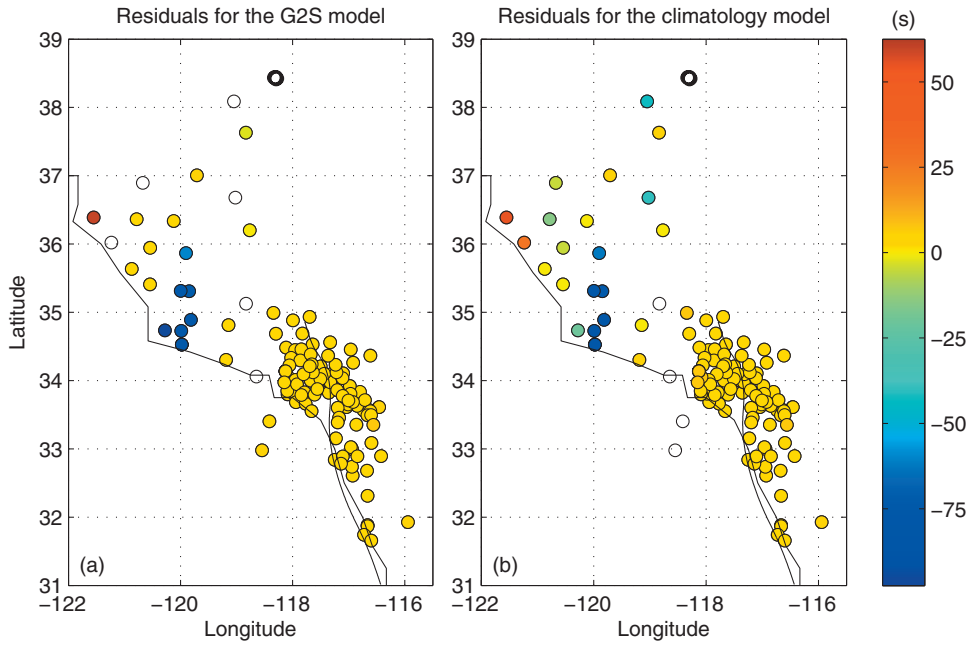

FIG. 12. Travel time residuals, in seconds, for atmospheric specifications based on the (a) G2S model and (b) climatology data. Positive residual values indicate that predicted arrival times are too late; negative residuals indicate that predicted arrival times are earlier than observed. Empty circles indicate stations at which observations were made but have no associated predictions for the given ray density used for computation of travel time predictions.

51–58 s for both atmospheric models. The predicted arrival times are consistent with the second arrival at that station, as shown in Fig. 8. Contrary to observations, both models predict that the Nevada stations are not far enough to the west to observe infrasound arrivals.

A significant feature of these results is the excellent agreement between predicted and observed arrival times for stations in regions where ray densities are predicted to be high. On average, observed arrival times were early by 2.6 s in these regions.

VI. DISCUSSIONS AND CONCLUSIONS

The supersonic descent of Atlantis above an area occupied by the USArray and other seismic networks on June 22, 2007 yielded an opportunity to evaluate atmospheric propagation modeling capabilities over a wide spatial, although not temporal region. The seismic networks across northern Mexico, California, and Nevada represented a 100- fold increase in station density over the available infrasound site density. The greater station availability for stations outside the primary sound carpet averted the usual difficulty of associating a seismic or infrasound signal with a particular event. For this reason, we were able to associate infrasound signals recorded on seismic sensors with Atlantis to distances of 400 km from the nearest point on the shuttle trajectory.

Comparison of predicted versus observed travel times shows agreement over much of the study area, as discussed in Sec. V. For the G2S model, travel time residuals are small within regions that are highly ensonified, as predicted by ray theory. This implies that the source model, infrasound propagation model, and G2S atmospheric specifications are adequate for predicting arrival times within these regions. It should be noted, however, that the agreement between observed and predicted arrival times at distances beyond a ground reflection point may have been somewhat fortuitous as we ignored terrain effects. In reality, scattering or deflection may occur at the reflection point if the ground surface is rough.

The results also suggest that the use of geometrical acoustics is inaccurate in computing arrival times where very low ray densities are predicted and, clearly, also within shadow zones. This is supported by the fact that ray theory relies on a high frequency approximation to wave propagation, which is valid when sound speeds vary on a scale length much larger than the propagation wavelength. This approximation starts to break down at infrasonic frequencies for typical atmospheric conditions. A more complete description of infrasound propagation includes finite wavelength effects such as diffraction, scattering (Embleton, 1996), and surface waves (Attenborough, 2002). These effects lead to much greater penetration of acoustic energy into shadow zones at amplitudes than predicted by ray theory (Embleton, 1996; Attenborough, 2002). This argument is further supported by the fact that infrasound detections have also been reported at distances of up to tens of kilometers within areas predicted by ray theory to be shadow zones (e.g., Ottemöller and Evers, 2008).

The small positive bias in the arrival time residuals within the shuttle's primary sound carpet indicates either a source effect or a bias in the adiabatic sound speeds. Potential errors in the source model point to a slight overestimate of the arrival times. First, there may be an error in the shape of the Mach cone used in our modeling. Equation (9.74) of (Whitham, 1974) indicates that at high Mach numbers, the true Mach cone angle is slightly greater than the simplifying assumption of $\alpha = \sin^{-1}(c/v)$ used here. This would lead to a different take-off angle from the Mach cone. Second, infrasound propagation near the shuttle is nonlinear as the result of increased sound speeds from the local overpressure. However, these effects on the order of several tenths of a second are not enough to account for the average 2.6 s bias observed. The bias in the adiabatic sound speeds within the atmosphere would have to be on the order of 5 m/s to yield the observed arrival times.

Finally, note that relatively small variations in the wind speed profiles can yield significant variations in predicted infrasound propagation. As shown in Fig. 2, the climatological wind speed profiles are smoother than those based on the G2S model. This yields differences in the pattern of ensonification at the ground level as shown in Fig. 6; highly ensonified regions are broader for the climatological model and extend along a line farther to the north-NW than for the G2S model. Several stations lie in the predicted acoustic shadow zone just beyond this line, including the Nevada stations where stratospheric arrivals were observed by both sensors. Instantaneous uncertainties of the G2S specification in the stratosphere are on the order of 10–15 m/s. This uncertainty may be sufficient to account for the lack of arrival time predictions for stations to the north-NW as well as the mismatch of the predicted surface skip locations of the stratospheric rays. More generally, insonification of the shadow zone could be due to scattering or refraction by small scale atmospheric inhomogeneities. The inhomogeneities have scale lengths comparable to infrasonic wavelengths and have been shown to affect infrasound propagation to large distances from a source (Kulichkov *et al.*, 2004).

ACKNOWLEDGMENTS

We thank J. F. Zumberge of the Jet Propulsion Laboratory and S. V. Murray of the Johnson Space Center for the shuttle time and position data. The NVIAR (infrasound) data were provided by the U.S. Army Space and Missile Defense Command. Support for the NVIAR station comes from the Southern Methodist University and the National Center for Physical Acoustics at the University of Mississippi. We are grateful to Raul Castro Escamilla at CICESE for providing data from the Mexican seismic stations. This study benefited greatly from the Data Management System offered by the Inc. Research Institutions for Seismology. We would also like to thank the NASA Goddard Space Flight Center, Global Model and Assimilation Office, and the NOAA National Centers for Environmental Predication for making their numerical weather prediction (NWP) products available for this scientific research. The High-Performance Wireless Research and Education Network provided wireless network access to the infrasound sensors at PFO and Camp Elliott. We would like to thank our three anonymous reviewers for their constructive feedback. This work was funded by the U.S. Army Space and Missile Defense Command under the University of Mississippi Subcontract No. 07-08-013. Auxiliary support is also provided to NRL by the Office of Naval Research. We dedicate this work to Hank Bass.

Arrowsmith, S. J., Drob, D. P., Hedlin, M. A. H., and Edwards, W. (**2007**). "A joint seismic and acoustic study of the Washington State bolide: Observations and modeling," J. Geophys. Res. **112**, D09304.

Attenborough, K. (**2002**). "Sound propagation close to the ground," Annu. Rev. Fluid Mech. **34**, 51–82.

Balachandran, N., Donn, W., and Rind, D. (**1977**). "Concorde sonic booms as an atmospheric probe," Science **197**, 47–49.0036-8075

Bloom, S., da Silva, A., Dee, D., Bosilovich, M., Chern, J.-D., Pawson, S., Schubert, S., Sienkiewicz, M., Stajner, I., Tan, W.-W., and Wu M.-L. (**2005**). "Documentation and validation of the goddard earth observing system (GEOS) data assimilation system—Version 4," NASA Report No. TM-2005-104606, Technical Report Series on Global Modeling and Data Assimilation, Greenbelt, MD.

Cates, J. E., and Sturtevant, B. (**2002**). "Seismic detection of sonic booms," J. Acoust. Soc. Am. **111**, 614–628.

Cochran, E. S., and Shearer, P. M. (**2006**). "Infrasound events detected with the southern California seismic network," Geophys. Res. Lett. **33**, L19803.

Drob, D. P., Picone, J. M., and Garces, M. (**2003**). "Global morphology of infrasound propagation," J. Geophys. Res. **108**, ACL13.1–ACL13.12.0148-0227

Embleton, T. F. W. (**1996**). "Tutorial on sound propagation outdoors," J. Acoust. Soc. Am. **100**, 31–48.

Evers, L. G., and Haak, H. W. (**2007**). "Infrasonic forerunners: Exceptionally fast acoustic phases," Geophys. Res. Lett. **34**, L10806.

Gibbons, S., Ringdal, F., and Kvaerna, T. (**2007**). "Joint seismic-infrasonic processing of recordings from repeating source of atmospheric explosions," J. Acoust. Soc. Am. **122**, EL158–EL164.

Hedin, A. E., Fleming, E. L., Manson, A. H., Scmidlin, F. J., Avery, S. K., Clark, R. R., Franke, S. J., Fraser, G. J., Tsunda, T., Vial, F., and Vincent, R. A. (**1996**). "Empirical wind model for the upper, middle, and lower atmosphere," J. Atmos. Terr. Phys. **58**, 1421–1447.0021-9169

Ishihara, Y., Furumoto, M., Sakai, S., and Tsukada, S. (**2004**). "The 2003 Kanto large bolide's trajectory determined from shockwaves recorded by a seismic network and images taken by a video camera," Geophys. Res. Lett. **31**, L14702.0094-8276

Kalnay, E., Kanamitsu, M., and Baker, W. E. (**1990**). "Global numerical weather prediction at the National Meteorological Center," Bull. Am. Meteorol. Soc. **71**, 1410–1428.

Kanamitsu, M. (**1989**). "Description of the NMC global data assimilation and forecast system," Weather Forecast. **4**, 335–342.0882-8156

Kanamori, H., Mori, J., Anderson, D. L., and Heaton, T. H. (**1991**). "Seismic excitation by the space shuttle Columbia," Nature (London) **349**, 781–782.0028-0836

Kanamori, H., Mori, J., Sturtevant, B., Anderson, D. L., and Heaton, T. H. (**1992**). "Seismic excitation by space shuttles," Shock Waves **2**, 89–96.

Kulichkov, S. N. (**2004**). "Long-range propagation and scattering of low-frequency sound pulses in the middle atmosphere," Meteorol. Atmos. Phys. **85**, 47–60.0177-7971

Langston, C. (**2004**). "Seismic ground motions from a bolide shock wave," Geophys. Res. Lett. **109**, B12309.0094-8276

Le Pichon, A., Garces, M., Blanc, E., Barthelemy, M., and Drob, D. P. (**2002**). "Acoustic propagation and atmosphere characteristics derived from infrasonic waves generated by the Concorde," J. Acoust. Soc. Am. **111**, 629–641.

Liszka, L. (**1978**). "Long-distance focusing of concorde sonic boom," J. Acoust. Soc. Am. **64**, 631–635.

Meltzer, A., Rudnick, R., Zeitler, P., Levander, A., Humphreys, G., Karlstrom, K., Ekström, G., Carlson, R., Dixon, T., Gurnis, M., Shearer, P., and van der Hilst, R. (**1999**). "USArray initiative," GSA Today **9**, 8–10.1052-5173

Millet, C., Robinet, J.-C., and Roblin, C. (**2007**). "On using computational aeroacoustics for long-range propagation of infrasounds in realistic atmospheres," Geophys. Res. Lett. **34**, L14814.0094-8276

Ostashev, V. E., Hohenwarter, D., Attenborough, K., Blanc-Benon, P., Juve, D., and Goedecke, G. H. (**2001**). "On the refraction law for a sound ray in a moving medium," Acta Acust. **87**, 303–306.

Ottemöller, L., and Evers, L. G. (**2008**). "Seismo-acoustic analysis of the buncefiled oil depot explosion in the UK, 2005 December 11," Geophys. J. Int. **172**, 1123–1134.

Picone, J. M., Hedin, A. E., Drob, D. P., and Aiken, A. C. (**2002**). "NRLMSIS-00 empirical model of the atmosphere: Statistical comparisons and scientific issues," J. Geophys. Res. **107**, 1468.

Silver, P. G., and Chan, W. W. (**1991**). "Shear-wave splitting and subcontinental mantle deformation," J. Geophys. Res. **96**, 16429–16454.0148-0227

Sutherland, L. C., and Bass, H. E. (**2004**). "Atmospheric absorption in the atmosphere up to 160 km," J. Acoust. Soc. Am. **115**, 1012–1032.

Thompson, R. J. (**1972**). "Ray theory for an inhomogeneous moving medium," J. Acoust. Soc. Am. **51**, 1675–1682.

Whitham, G. B. (**1974**). *Linear and Nonlinear Waves* (Wiley, New York).

Zumberge, M. A., Berger, J., Hedlin, M. A. H., Hilt, R., Nooner, S., and Widmer-Schnidrig, R. (**2003**). "An optical fiber infrasound sensor: a new lower limit on atmospheric pressure noise between 1 Hz and 10 Hz," J. Acoust. Soc. Am. **113**, 2474–2479.